**32nd Electric Vehicle Symposium (EVS32)**
**Lyon, France, May 19-22, 2019**

# Electric and Conventional Vehicle Performance over Eco-Driving Cycles: Energy Benefits and Component Loss

Zhiming Gao[1], Tim J. LaClair

*Oak Ridge National Laboratory, P.O. Box 2008, Oak Ridge, TN 37831*

*[1]Corresponding author: gaoz@ornl.gov*

**Executive Summary**

Battery electric vehicles (BEVs) are expected to be a pathway towards meeting greenhouse and criteria pollutant gas reductions in the current and future transportation sector. However, BEV technologies are still evolving, including efficiency optimization and enhancement. Emerging connected and automated vehicle (CAV) technologies provide an in-depth insight for developing innovative applications and systems to leverage BEV energy efficiency and substantially transform transportation systems. Therefore, we present simulation studies of various BEV types and compare the performance between measured, real-world drive cycles and highly optimized eco-driving cycles that are representative of trajectory modifications using advanced CAV technologies. The investigated vehicles include a compact car and a Class 7 delivery truck. The results demonstrate that eco-driving has a high potential to reduce energy consumption for the BEVs considered. As part of the study, a comprehensive EV powertrain model was developed to account for key EV components and powertrain configurations. The impact of eco-driving was further evaluated for conventional vehicles with characteristics that are comparable to the modeled BEVs.

*Keywords: electric vehicle, eco-driving, component efficiency, powertrain modeling*

## 1 Introduction

US Transportation is responsible for over 3 trillion vehicle-miles driven annually, 11 billion tons of freight transported, and 70% of the nation's petroleum consumption. The transportation sector also significantly impacts air pollution and climate change [1]. Consequently, battery electric vehicles (BEVs) are considered to be a critical pathway towards achieving energy independence and greenhouse and criteria pollutant gas reduction goals for both current and future transportation [2]. To enhance the energy efficiency and market penetration of BEVs, extensive work has been carried out, particularly for BEV components, powertrain control and energy management [3]. On the other hand, innovative technologies for automation and connectivity are becoming more and more attractive for integration with the control strategy of BEVs. In particular, connectivity, automation, and electrification are considered as three major pillars supporting a more efficient future transportation system and cleaner environment. Therefore, it is desirable to adopt connected and automated vehicle (CAV) technologies for optimized BEV performance via eco-driving functions, particularly for boosting BEV energy efficiency, driving range and market adoption [3].

One effective eco-driving technology is the eco-Approach and Departure (EAD) application, which uses traffic signal phase and timing (SPaT) information from upcoming traffic signals along with information about the equipped vehicle and preceding traffic to determine the most energy efficient speed trajectory to pass through an intersection [4-6]. Real-road tests have shown that EAD is expected to significantly reduce or eliminate braking, as well as yielding benefits in traffic throughput. In 2010, the NHTSA performed a preliminary analysis on the benefits of SPaT and EAD, showing a 90% reduction in red light violations and up to 35% in energy savings for light-duty (LD) vehicles [7]. The University of California Riverside utilized a 2008 Nissan Altima to test an EAD application in Real-World Traffic, indicating 6% energy savings for trip segments under light traffic conditions, as well as substantial CO/HC/NOx emissions reduction [4]. Meanwhile, substantial simulations confirm the benefits of the EAD application. For example, a simulated eco-driving system for an isolated signalized intersection enabled engine-powered LD vehicles to achieve from 2.02% to 58.01% in fuel savings and from 1.97% to 33.26% in $CO_2$ emissions reduction [8]; Heavy-duty (HD) truck EAD algorithms for a signalized intersection have also been explored, showing up to 16% fuel saving [5]. All these reported results are based on vehicles powered by conventional combustion engines. For BEVs, similar studies have been conducted to evaluate battery energy savings under EAD driving modes. Qi et.al evaluated the energy synergies of combining vehicle connectivity, automation and electrification, by simulating an EAD system for BEVs with real-road driving data [9]. Zhang and Yao [10] simulated that BEVs following an eco-driving strategy at signalized intersections achieved at least 8.01% in energy savings relative to normal driving conditions, which was assessed using a microscopic, driving parameters-based energy consumption model based on chassis dynamometer testing data. Flehmig et al. [11] reported an adaptive cruise control (ACC) simulation for estimating a BEV's energy-optimal trajectory when following another vehicle in traffic, and the result showed a 2-4% saving compared to regular traffic conditions. However, none of the studies available in the public domain address how eco-driving impacts BEV component performance and efficiencies. There is currently inadequate information to further improve BEV component and powertrain performance under eco-driving conditions. Nonetheless, these are particularly important and attractive considerations for OEMs and automotive Tier 1 suppliers in designing and optimizing BEV components and powertrain systems for future BEVs.

To address the issues identified above, we present a simulation study for selected LD/HD BEV types and compare their performance when driving on typical real-road drive cycles to that when following optimized eco-driving cycles that comprise CAV-based eco-driving technologies such as EAD. The BEVs considered include a compact vehicle and a Class 7 delivery truck. The type of driving evaluated includes city conditions for the compact vehicle and mixed highway driving conditions for the trucks. In addition, the results are compared to those of comparable conventional vehicles in order to fully understand the impact of eco-driving on vehicle component and powertrain system performance. As part of the study, a BEV powertrain model was established to account for key BEV components and powertrain configurations. The BEV powertrain model employs data and models available from the public domain, as well as some existing ORNL component models, measurement data, and models adapted from Autonomie software [12].

# 2 Methodology and assumptions

## 2.1 BEV powertrain model

A comprehensive BEV model has been developed to describe key BEV components that impact driving efficiency: battery, motor, final drive, wheel, chassis, and accessory loads. A schematic of the model structure is presented in Fig. 1.

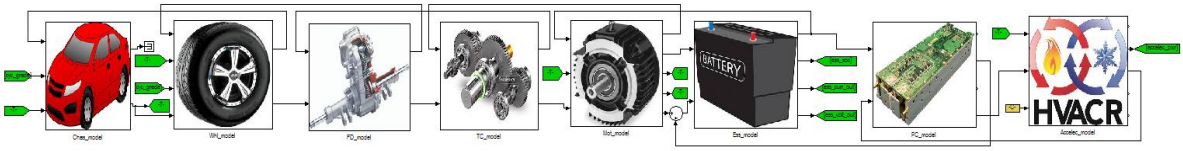


Figure1. The powertrain model configuration accounting for key BEV components.

### 2.1.1 Tractive force methodology

To evaluate the impact of acceleration, aerodynamic loss, rolling resistance and road grade on vehicle energy consumption, the tractive force required at any time is given as follows [13-14]:

$$F_{tract} = m \cdot \frac{dV}{dt} + \frac{1}{2}\rho \cdot C_d \cdot A_f \cdot V^2 + m \cdot g \cdot C_{rr} \cdot \cos\theta + m \cdot g \cdot \sin\theta \quad (1)$$

where $F_{tract}$ is the required vehicle tractive force; $V$ is vehicle velocity; $\rho$ is air density; $C_d$ is the aerodynamic drag coefficient; $C_{rr}$ is the rolling resistance coefficient; $A_f$ is the projected frontal area; $\theta$ is the road grade; and $m$ is the vehicle mass. $g$ is gravity; $t$ is time. The evaluation of aerodynamic drag, rolling resistance, and road grade on the EV tractive force demand is addressed in the chassis and wheel component modules shown in Figure 1.

### 2.1.2 Electric motor and inverter model

A map-based performance model was used to account for the energy consumption of the electric motor and inverter over the entire motor operating conditions [3]. The map-based model adopts the efficiency maps of motors and inverters, which were generated from experimental data measured under steady-state conditions over a pre-defined matrix of speed and torque combinations. Figure 2 shows the combined efficiency of the Nissan Leaf's motor and inverter. In the map-based model, the motor's output mechanical power is estimated based on motor speed and torque; the inverter's input electrical power are estimated using the motor's output mechanical power devided by combined motor and inverter efficiency. The inverter input electrical power is assumed to be equivalent to the battery power output. The curve for the motor torque boundary shown in Figure 2 is $\tau_{mot,pos\_bdry}$, and the motor regeneration torque boundary is assumed to be $\tau_{mot,neg\_bdry} = -\tau_{mot,pos\_bdry}$. In addition, the electric motor and inverter model include a simple factor for scaling the power and torque outputs of simulated motors and inverters based on maintaining the equivalent performance efficiency and speed range. This strategy allows scaling up or down the available motor maps to approximate motor performance maps for larger or smaller motors, whose maps may be not available, with reasonable accuracy.

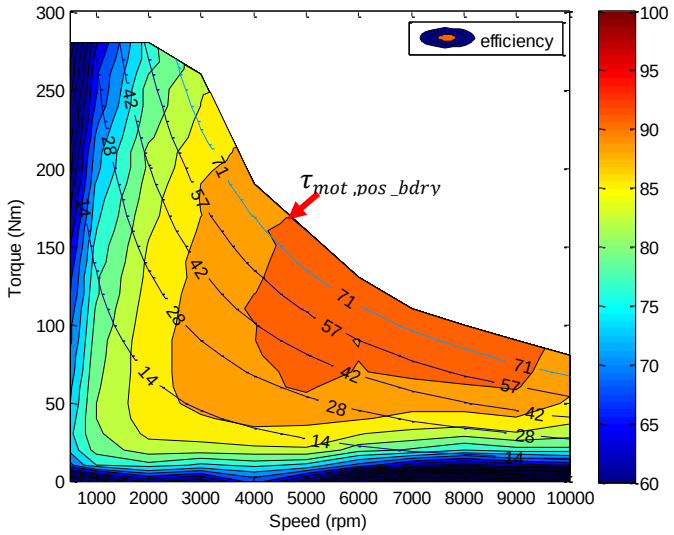


Figure 2: The combined efficiency map of Nissan leaf motor and inverter, rated at 280Nm torque and 80 kW power, which was tested at ORNL under 375V DC-link voltage and 65ºC steady-state cooling temperature [15].

### 2.1.3 Li-ion battery model

The battery package is modeled based on an equivalent circuit of multiple serial and parallel battery cells, each of which is assumed to have the same performance. In the single battery cell modeling, an RC-based equivalent-circuit battery cell dynamic model was considered to account for key transient response physics using electrical circuit analog components based on the electrical network consisting of a series resistor and two RC parallel networks, as shown in Fig. 3. The RC parallel networks represent short- and long-time step responses. On the basis of experimental results, the use of two RC networks, as opposed to one or three, provides the best tradeoff between accuracy and complexity [3]. The considered components include voltage

sources, variable resistors, and capacitors. The equivalent-circuit model accounts for open-circuit voltage, ohmic resistances in the connector, electrodes and electrolyte, and two sets of parallel resistor-capacitor combinations to reproduce the effects of mass transport and the electric double layer, respectively. In addition, the impact of temperature and charging/discharging rate on battery SOC are also considered. The details are described in Eqs. 2(a)-2(e). Based on the required overall battery package capacity and voltage, an appropriate combination of series and parallel connections is determined to simulate the complete vehicle battery module, as shows in Figure 3 and Eqs. 2(f)-2(g).

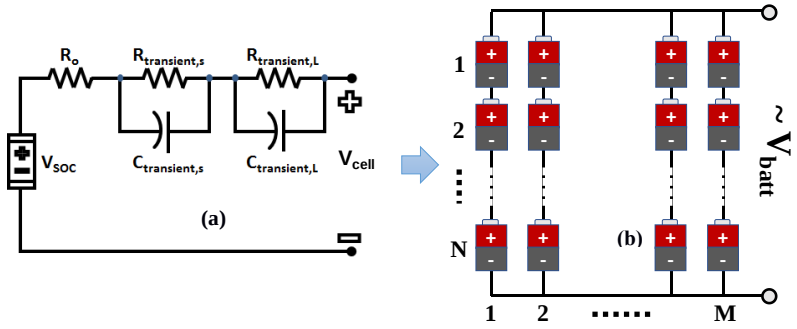


Figure 3. An equivalent-circuit battery cell dynamic model for simulating a battery package comprised of multiple serial and parallel battery cells. (a) single battery cell configuration; (b) battery package configuration.

$$\frac{dV_{tran,L}}{dt} = \frac{I_{cell}}{C_{tran,L}} - \frac{V_{tran,L}}{R_{tran,L} \cdot C_{tran,L}} \tag{2a}$$

$$\frac{dV_{tran,S}}{dt} = \frac{I_{cell}}{C_{tran,S}} - \frac{V_{tran,S}}{R_{tran,S} \cdot C_{tran,S}} \tag{2b}$$

$$V_{cell} = V_{SOC} - I_{cell} \cdot R_o - V_{tran,L} - V_{trans,S} + \Delta\varepsilon(T_{cell}) \tag{2c}$$

$$m_{cell} C_{pcell} \frac{dT_{cell}}{dt} = I_{cell} \cdot R_o + \frac{V_{tran,L}^2}{R_{tran,L}} + \frac{V_{tran,S}^2}{R_{tran,S}} - hA(T_{cell} - T_{amb}) \tag{2d}$$

$$SOC = \frac{1}{C_{cell}} \int \alpha(I_{cell}) \beta(T_{cell}) I_{cell} dt \tag{2e}$$

$$V_{batt} = N_{series} \cdot V_{cell} \tag{2f}$$

$$I_{batt} = M_{parallel} \cdot I_{cell} \tag{2g}$$

where $V_{SOC}$ is the open circuit voltage which is a nonlinear function of SOC and normally measured as the steady-state open circuit terminal voltage at various SOC points; $V_{tran,S}$ and $V_{tran,L}$ are voltages of short- and long-time step responses of RC networks, respectively; $R_{tran,S}$, $R_{tran,L}$, $C_{tran,S}$, and $C_{tran,L}$ represent short- and long-time constants of the step response of RC networks; $R_o$ is a series resistor; $V_{cell}$ and $I_{cell}$ are the battery cell output voltage and current; $V_{batt}$ and $I_{batt}$ are the modeling voltage and current of the overall battery package with $N_{series}$ battery cells in series and $M_{parallel}$ battery cells in parallel; $\Delta\varepsilon$ is a temperature-dependent potential-correction term for the battery; $\alpha(I_{cell})$ is a charging/discharging rate factor; $\beta(T_{cell})$ is a temperature factor; $T_{cell}$ and $T_{amb}$ are battery cell and ambient temperature; $m_{cell}C_{pcell}$ and $hA$ are battery cell mass capacity and heat transfer rate, respectively.

$V_{SOC}$, $R_{tran,S}$, $R_{tran,L}$, $C_{tran,S}$, and $C_{tran,L}$, as well as $\Delta\varepsilon(T_{cell})$ , $\alpha(I_{cell})$, and $\beta(T_{cell})$, depend on individual battery type, design, and fabrication. $V_{SOC}$, $R_{tran,S}$, $R_{tran,L}$, $C_{tran,S}$, and $C_{tran,L}$ are functions of SOC. $\Delta\varepsilon(T_{cell})$ , $\alpha(I_{cell})$, and $\beta(T_{cell})$ are impacted by the battery cell current and temperature. All of them can be derived from battery test data.

### 2.1.4 Driver, drivetrain components and control model

A driver model was used to control vehicle operation. A proportional-integral (PI) control methodology was used to manage the gap between the real and targeted vehicle speeds. The driver's wheel torque demand is calculated based on Eq. 3.

$$\tau_{wh,drv} = F_{tract} R_{wh} + K_P \cdot \Delta V + K_I \cdot \int \Delta V dt \tag{3}$$

In Eq. 3, $\tau_{wh,drv}$ is driver wheel torque demand; the values of $K_p$ and $K_I$ are constants for the PI speed control and depend on the driver behavior and the simulated vehicle system; $R_{wh}$ is the effective wheel rolling radius; $\Delta V = V_{target} - V_{drv}$; $V_{target}$ and $V_{drv}$ are the targeted and simulated driving vehicle speeds, respectively.

Then, $\tau_{wh,drv}$ is used to determine motor and braking torque demand, $\tau_{mot,dmd}$ and $\tau_{brk,dmd}$, respectively. However, at vehicle acceleration, the motor torque demand is determined by not only driver acceleration demand $\alpha_{acc,drv}$, but also is limited by the operating boundary of the motors and batteries. The motor torque demand is thus defined by the boundary constraints of motor acceleration and battery power output.

$$\tau_{mot,dmd} = \min\left(\frac{\tau_{wh,drv}}{R_{tc}\cdot R_{fd}}, \frac{W_{batt,dischg\_bdry} - W_{acc,elec}}{\omega_{mot}}, \tau_{mot,accel\_bdry}\right) \forall\left(\tau_{wh,drv} > 0\right) \quad (4a)$$

Similarly at vehicle braking, the braking torque and motor regenerative torque demands are dependent on the constraints of the regenerative conditions, as well as motor and battery operation boundaries, as given below. Both the motor regenerative and braking torque demands are negative during vehicle braking.

$$\tau_{mot,dmd} = \max\left(\frac{\tau_{wh,drv}\cdot\delta_{spd}\cdot\delta_{dec}}{R_{tc}\cdot R_{fd}}, \frac{W_{batt,chg\_bdry} - W_{acc,elec}}{\omega_{mot}}, \tau_{mot,regen\_bdry}\right) \forall\left(\tau_{wh,drv} < 0\right) \quad (4b)$$

and

$$\tau_{brk,dmd} = \max(\tau_{wh,drv} - \tau_{mot,dmd}\cdot R_{tc}\cdot R_{fd}, 0) \forall\left(\tau_{wh,drv} < 0\right) \quad (4c)$$

Therefore, the forward-looking driving speed of the simulated vehicle is described using the equation below.

$$\frac{dV_{drv}}{dt} = \frac{\tau_{mot,dmd}\cdot\eta_{fd}\cdot\eta_{tc}\cdot R_{fd}\cdot R_{tc}}{\left(m + I_{tot}/R_{wh}^2\right)\cdot R_{wh}} - \frac{1}{\left(m + I_{tot}/R_{wh}^2\right)}\left(\frac{1}{2}\rho C_d A_f V_{drv}^2 + mgC_{rr}\cos\theta + mg\sin\theta\right) + \frac{\tau_{brk,dmd}}{\left(m + I_{tot}/R_{wh}^2\right)\cdot R_{wh}} \quad (5)$$

In Eqs. (4)-(5), $W_{batt,chg\_bdry}$ and $W_{batt,dischg\_bdry}$ are the battery charging and discharging power boundary, respectively; $R_{fd}$ is the final drive ratio; $R_{tc}$ is the torque coupler ratio; $\delta_{spd}$ and $\delta_{dec}$ are factors that consider the constraints during brake regeneration. The constraints are used to distinguish vehicle emergency braking from regenerative kinetic energy and avoid very low kinetic energy regeneration. $W_{acc,elec}$is the electric accessory load, which is taken to be constant. $I_{tot}$ addresses the total inertia of the powertrain.

## 2.2 BEV configurations and model validation

Two BEV powertrain configurations were specified to account for a LD compact car and HD delivery truck, respectively. The LD electric car model was created based on a Nissan Leaf configuration, for which the motor map was generated from measurements of a 2012 Nissan Leaf motor rated at 80 kW (see Figure 2). The specification of the motor and battery for the HD E-truck model were estimated based on ORNL's commercial vehicle electrification evaluation tool (CVEET) [16-17] which is a framework tool for commercial vehicle electrification. To confirm that the simulated vehicles reasonably reflect the performance of electric vehicles, the LD BEV simulations were carried out using the current model and compared with the chassis dyno data of a 2012 Nissan Leaf following the regular urban dynamometer driving schedule (UDDS), as collected by Argonne National Laboratory. For the city drive cycle of 12 km and 1372s, the predicted and measured battery energy consumption were 125.5 Wh/km and 129.8 Wh/km, respectively. The simulation error is less than 4%. Furthermore, the predicted transient motor performance also matches very well with the measurement of both motor speed and torque (see Figure 4). The results indicate that the assumptions employed for the EV powertrain model were reasonable. We do not have appropriate experimental data for the validation of the E-Truck model directly. Alternatively, simulation results from Autonomie software were used to validate and compare with our models. Results indicated less than 5% difference, implying that the E-Truck assumptions are also acceptable. The key parameters for the two BEVs are listed in Table 1.

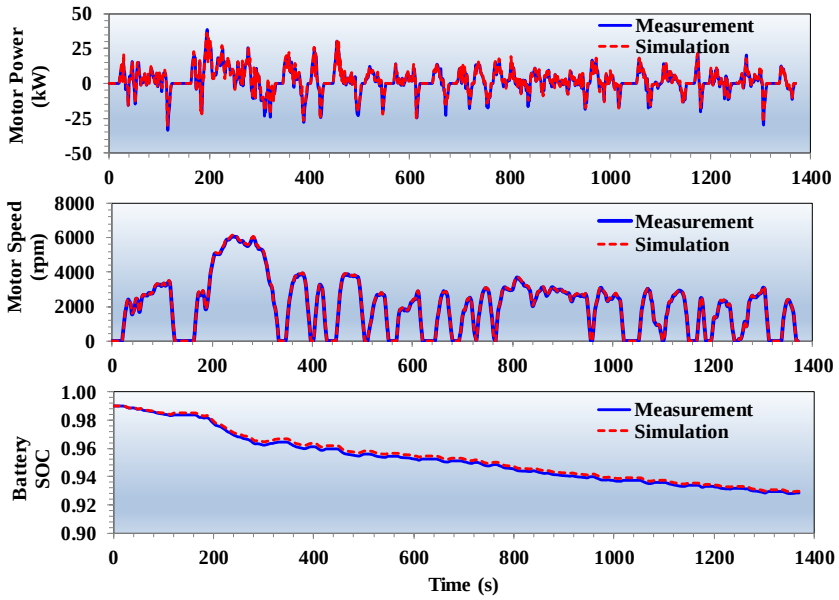


Figure 4: Comparison of motor power, speed and battery SOC for the simulated LD BEV over the cold-start UDDS cycle.

Table 1: Specifications of electrical vehicle components and key parameters.

| Component | Parameters | LD BEV | Electric Truck |
|---|---|---|---|
| Aerodynamic drag coeff. | Cd | 0.32 | 0.62 |
| Rolling resistance coeff. | Crr | 0.007 | 0.009 |
| Frontal Area | $A_f$ ($m^2$) | 2.01 | 9.0 |
| Wheel tire | Wheel radius (m) | 0.3125 | 0.53 |
| | Inertia (kg-$m^2$) | 0.25 | 1.0 |
| Final drive | Final ratio | 7.94 | 7.94 |
| | Inertia per wheel tire (kg-$m^2$) | <0.01 | <0.01 |
| Torque coupler | TC ratio | 1.01 | 1.6 |
| | Inertia (kg-$m^2$) | <0.01 | <0.01 |
| Motor | Max power (kW) | 84 | 265 |
| | Continuous power (kW) | 42 | 132 |
| | Max torque (Nm) | 280 | 874 |
| | Inertia (kg-$m^2$) | 0.03 | 0.08 |
| Battery | Capacity (kWh) | 24 | 265 |
| | Peak chg power (kW) | 148 | 1500 |
| | Peak dis power (kW) | 140 | 1580 |
| | Normal Voltage (V) | 374 | 581 |
| Electric accessory | Constant power (kW) | 0.2 | 4.0 |
| Vehicle mass | Mass (kg) | 1515 | 15434 |

## 2.3 Eco-driving methodology

A simplified eco-driving model was developed that provides similar speed profiles to an EAD application by employing coasting at appropriate locations to minimize braking. The approach calculates an appropriate coasting speed profile prior to the vehicle arriving at locations where braking is required at stops or traffic signals. This coasting solution can be evaluated from any starting location and speed, but different end points or times will of course be obtained for different starting locations. Details of the method are provided in [3].

Two relevant driving cycles were selected based on on-road measurement data for a compact car and a delivery truck. The passenger car case is a city driving cycle with a total length of 17.5 km. The regional delivery cycle is a combined highway and city driving cycle that is 92.7 km long. The proposed eco-driving methodology is used to create optimized eco-driving drive cycles which are used to estimate the potential benefits of eco-cruise and traffic signal EAD applications using detailed powertrain simulations.

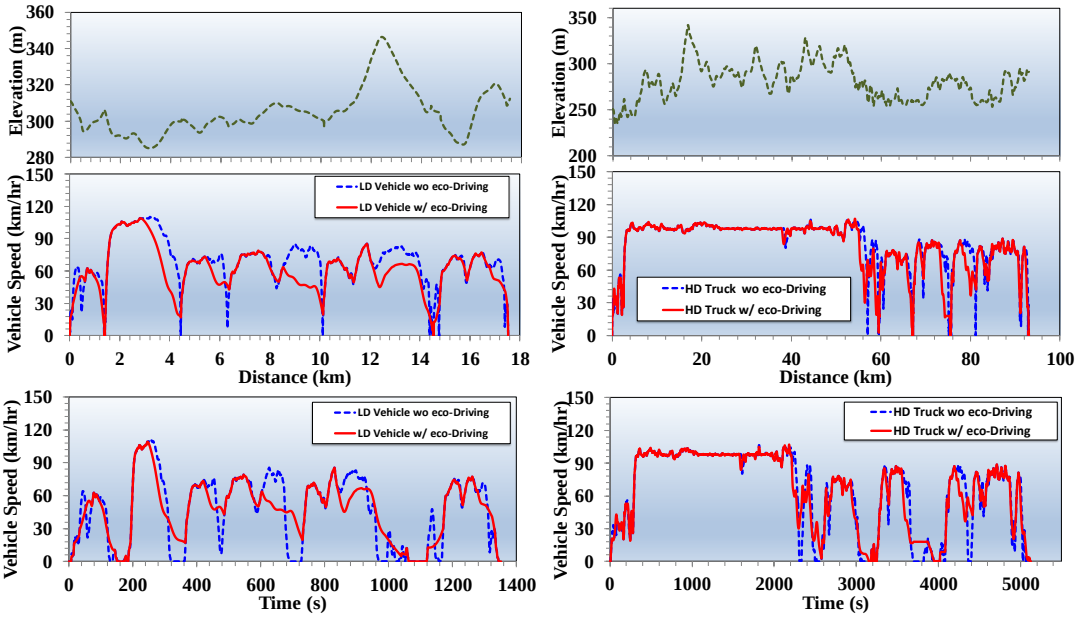


(a) LD car (b) HD Truck

Figure 5: Passenger car and delivery truck speed profiles with and without eco-driving, including elevation profile vs. distance, speed profile vs. distance, and speed profile vs. time.

Figures 5 show the comparison of the original driving cycle and the eco-driving cycles. It is clear that the three eco-driving cases representing the EAD application eliminate stops significantly. In the eco-driving cycles, the braking tractive energy (the integral of all periods requiring braking power) is reduced by 65.4 and 70.8% for the passenger car and delivery truck, respectively; also, the propulsive tractive energy (integral of all positive tractive powers) is reduced by 32.7% and 12.9%, respectively, for the passenger car and delivery truck.

# 3 Results

## 3.1 BEV Simulations

In the simulated passenger BEV, the battery energy consumption with and without eco-driving was 107.0 Wh/km and 146.7 Wh/km, respectively. The eco-driving allows the simulated LD BEV to achieve 27% battery energy savings. The detailed component energy losses are shown in Fig. 6, revealing that the key component energy losses are aerodynamic drag, motor loss, rolling resistance, and drivetrain loss. Eco-driving reduces the motor loss by 51%, as well as the aerodynamic drag loss by 20% and the drivetrain loss by 50%, but eco-driving does not affect the rolling resistance loss. In addition, the eco-driving reduces the frictional braking loss by 65% and the battery loss by 39%, although the magnitude of these actual energy losses are relatively small compared to the four key component energy losses. There is a different mechanism for the frictional braking losses between the cases with and without eco-driving. Eco-driving reduces frictional braking loss by avoiding active decelerations using an appropriate speed control. The BEV without eco-driving, however, also has very low frictional braking loss as a result of braking regeneration. The latter transfers a portion of the regenerated kinetic energy to motor energy losses. Figure 6(b) confirms that the eco-driving operation eliminates most braking regen, which becomes nearly zero. The BEV operation without eco-driving regenerates braking energy, but the regeneration process effectively doubles the motor energy losses (i.e. energy loss takes place during regeneration and propulsion) for the portion of power that is

regenerated. This explains why the eco-driving enables a significant decrease in motor energy loss (see Figure 6(a) while boosting battery energy saving (see Figure 6(c)).

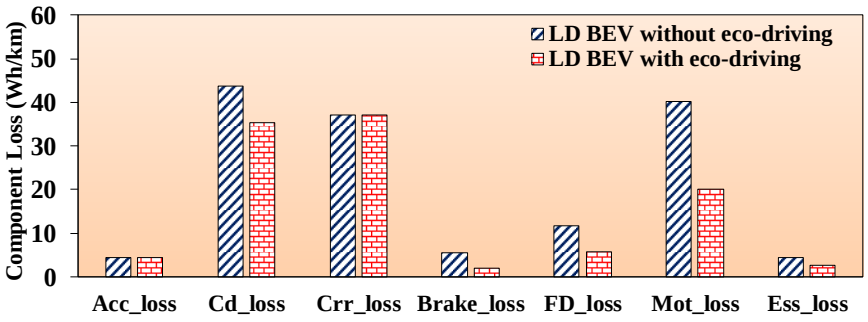


(a) Comparison of LD BEV component losses with vs. without eco-driving

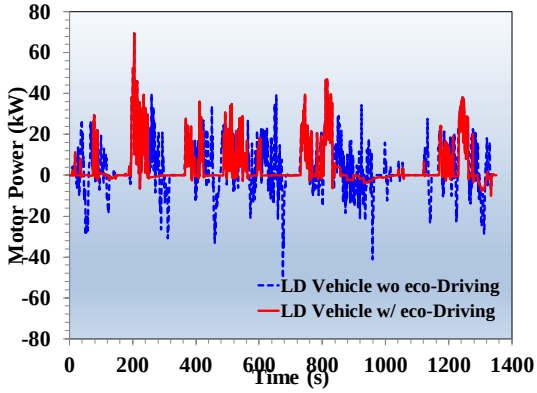


(b) Transient motor power

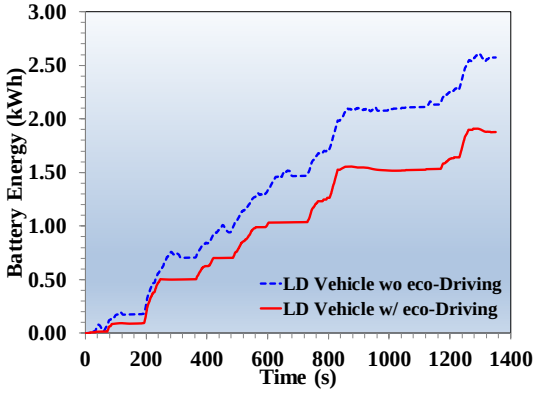


(c) Battery energy consumption

Figure 6. Comparison of the LD passenger BEV energy losses (a) with and without eco-driving; (b) transient motor power and (c) cumulative battery energy consumption

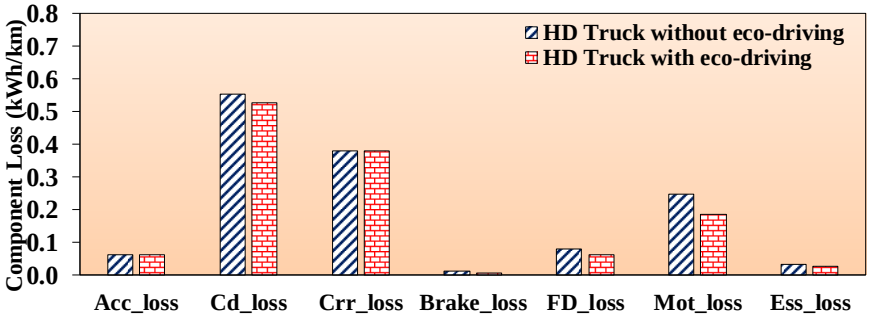


(a) Comparison of HD E-truck component losses with vs. without eco-driving

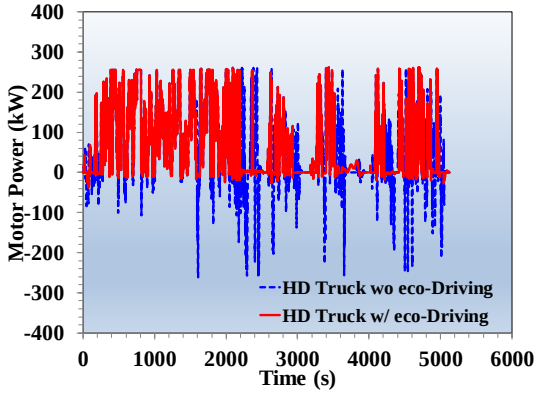


(c) Transient motor power

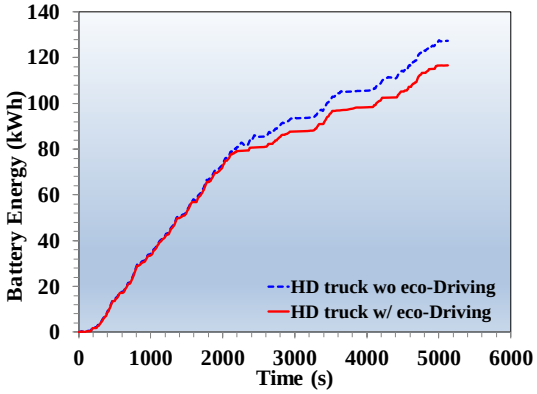


(d) Battery energy consumption

Figure 7. Comparison of the HD E-Truck energy losses (a) with or without eco-driving; (b) transient motor power and (c) cumulative battery energy consumption

The truck case shows a slightly different scenario for which the eco-driving optimized drive cycle results in an 8% battery energy savings (see figure 7). The battery energy consumption with and without eco-driving are 1.25 kWh/km and 1.37 kWh/km, respectively. The smaller benefit in this case is mainly because the delivery truck drives a significant distance on the highway (see the first 2000s shown in Figure 7), which does not provide substantial braking reduction opportunities. In the simulation, truck platooning is not considered. For the E-truck case, the top key component energy losses are aerodynamic drag, rolling resistance, motor loss, and final drive loss. The eco-driving decreases the motor loss by 25%, as well as the aerodynamic drag loss by 5% and the final drive loss by 25%, but eco-driving does not affect rolling resistance loss either. In the E-truck simulations, the braking loss associated with the limited delivery stops does not result in a substantial impact on the total energy consumption, since it represents less than 1% of the overall energy consumption in the original drive cycle.

## 3.2 Conventional Powertrain Vehicles and Comparison with BEVs

The impact of eco-driving on conventional vehicles was also studied to compare with similarly configured BEVs. Two conventional powertrain vehicle models were created using Autonomie [12] based on the basic vehicle parameters listed in Table 1. These conventional vehicle powertrain models developed using Autonomie have been described in detail in our previous studies [18-23]. The impact of eco-driving on the conventional vehicles is summarized in Figure 8. Briefly, eco-driving enables a rather significant reduction in the conventional vehicles' braking energy losses. Frictional braking is reduced by 89% and 88% in the conventional passenger car and HD truck on the eco-drive cycle, compared to 65% and 50% for the comparable E-car and E-truck, respectively. The difference in the absolute levels of frictional braking energy are also considerable since regenerative braking is not available for the conventional vehicles, hence their frictional braking losses are much greater than in the corresponding BEV cases. For the LD cass, the brkaing energy of conventional engine-powered vehicle and BEV is 43.2 Wh/km vs. 5.4 Wh/km without eco-driving and 4.7 Wh/km vs. 1.9 Wh/km with eco-driving, respectively; For the HD cass, the brkaing energy of conventional engine-powered truck and E-truck is 0.15 kWh/km vs. ~0.01 kWh/km without eco-driving and 0.02 kWh/km vs. >0.005 kWh/km with eco-driving, respectively.

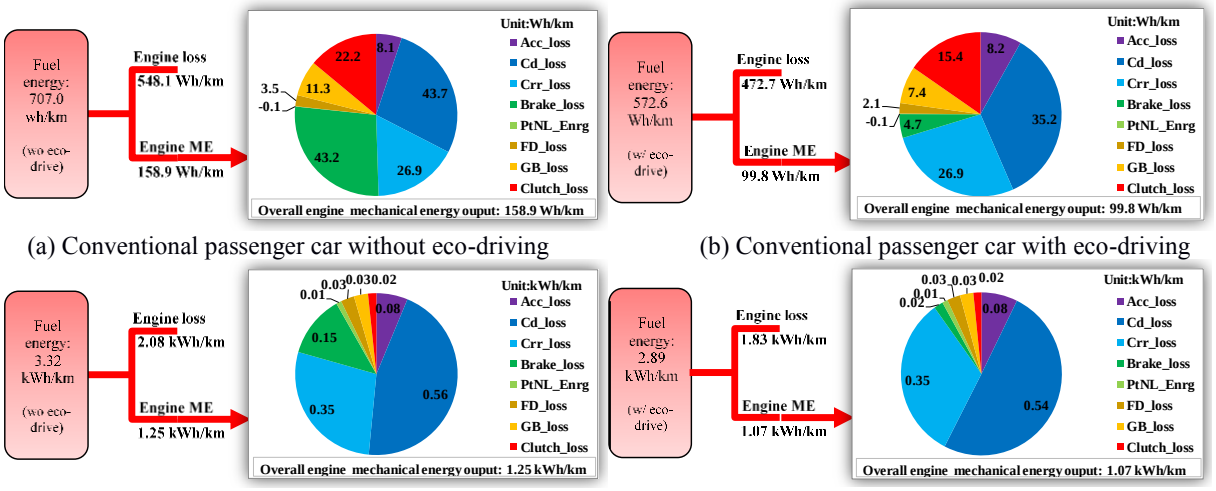


(a) Conventional passenger car without eco-driving

(b) Conventional passenger car with eco-driving

(c) Conventional HD truck without eco-driving

(d) Conventional HD truck with eco-driving

Figure 8: Energy consumption distribution of the (a)-(b) conventional passenger car and (c)-(d) delivery truck, with and without eco-driving.

The results also show that eco-driving leads to frequent engine operation at low loads, which generally corresponds to low efficiency. Figure 9 shows the detailed second-by-second fuel consumption and engine efficiency profiles. The engine average efficiencies are 22.4% without eco-driving vs. 17.0% with eco-driving for the conventional passenger car, and 37.4% without eco-driving vs. 36.9% with eco-driving for the conventional truck. For the conventional passenger car, the maximum potential of fuel energy savings is limited by low engine efficiency in spite of the greater reduction in mechanical energy output due to eco-driving. Thus, a Start/Stop technology with an Integrated Starter and Generator (ISG) can offer significant potential to boost the fuel energy savings in conventional engine-powered passenger cars with eco-driving.

This Stop/Go system would shut down the engine when the vehicle coasts down and completely stops, and then the ISG restarts the engine immediately when the driver pushes the accelerator. The conventional HD truck, on the other hand, still seems able to maximize the potential of fuel energy savings and engine mechanical energy output reduction simultaneously, although the benefits were found to be less than those of the conventional passenger car due to the delivery truck's driving pattern, which has much less-frequent stops.

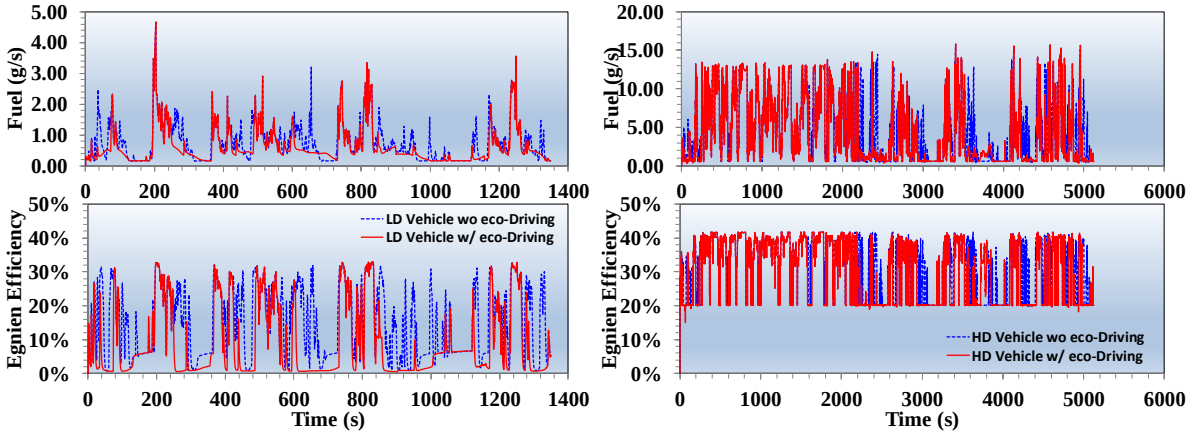


(a) LD car (b) HD Truck

Figure 9: Fuel consumption and engine efficiency profiles of conventional passenger car and delivery truck with and without eco-driving; passenger car: stoichiometric gasoline engine; delivery truck: lean-burn diesel engine.

# 4 Summary

A general EV simulation model that addresses component and system performance was developed to evaluate energy consumption and component performances of LD/HD battery electric vehicles. The simulations were carried out to identify the potential benefits of eco-driving for electrified cars and E-trucks. The results demonstrate that eco-driving boosts BEV energy savings and reduces motor component loss significantly. Eco-driving enables BEVs to virtually eliminate braking, which boosts the motor component loss reduction due to diminished regenerative braking. The dominant component losses of the EVs include aerodynamic drag, rolling resistance and drivetrain loss, in addition to motor loss.While the other significant component losses are reduced with eco-driving, it is noted that the optimized drive cycles do not impact the rolling resistance loss. Low rolling resistance tire technology can therefore have a significant impact on the efficiency of BEVs with eco-driving. The impact of eco-driving on conventional vehicles was also studied and compared to BEVs with similar size and performance characteristics. The observations show that eco-driving provides a much larger reduction in the conventional vehicles' braking energy loss compared to the comparable BEVs. However, eco-driving also leads to frequent engine operation at low loads, corresponding to lower efficiency, at least for non-highway driving conditions. As a result, the reduction in the conventional vehicle's energy consumption due to eco-driving is notably lower for the LD vehicle than would be expected from the mechanical energy reductions.

# Acknowledgments

This work was sponsored by the U.S. Department of Energy's Vehicle Technologies office and ARPA-E NEXT-CAR program. The authors thank our colleagues for their helpful suggestions and insights in this work.

# References


[1] Vehicle Technology Office. https://www.energy.gov/eere/vehicles/vehicle-technologies-office; 2018 Accessed 1 March 2019.

[2] Gao, Z, Lin Z, LaClair TJ, Liu C, Li JM, Birky AK, et. al. Battery Capacity and Recharging Needs for Electric Buses in City Transit Service. Energy, Vol. 122, 2017, 588-600.

[3] Gao Z, LaClair T, Ou S, Huff S, Wu G, Hao P, et al., Evaluation of electric vehicle component performance over eco-driving cycles. Energy, Vol. 172, 2019, 823-839. https://doi.org/10.1016/j.energy.2019.02.017.

[4] Hao P, Wu G, Boriboonsomsin K, Barth MJ. (2018). Eco-approach and departure (EAD) application for actuated signals in real-world traffic. IEEE Transactions on Intelligent Transportation Systems 2018; https://doi.org/10.1109/TITS.2018.2794509.

[5] Hao P, Boriboonsomsin K, Wang C, Wu G, Barth M. Connected eco-approach and departure (EAD) system for diesel trucks. TRB 18-06464, 2018.

[6] Fredette D, Ozguner U. Dynamic eco-driving's fuel saving potential in traffic: multi-vehicle simulation study comparing three representative methods. IEEE Transactions on Intelligent Transportation Systems 2018; 19(9): 2871-2879. https://doi.org/10.1109/TITS.2017.2766767.

[7] Huang X, Peng H. Speed trajectory planning at signalized intersections using sequential convex optimization. IEEE American Control Conference (ACC), 2017, pp. 2992-2997. https://doi.org/10.23919/ACC.2017.7963406.

[8] Jiang H, Hu J, An S, Wang M, Park BB, Eco approaching at an isolated signalized intersection under partially connected and automated vehicles environment, Transportation Research Part C 2017; 79: 290-307. https://doi.org/10.1016/j.trc.2017.04.001 .

[9] Qi X, Barth MJ, Wu G, Boriboonsomsin K, Wang P. Energy impact of connected eco-driving on electric vehicles. In: Meyer G, Beiker S editors. Road Vehicle Automation 4, Springer, Cham, 2018, pp. 97-111. https://doi.org/10.1007/978-3-319-60934-8_10.

[10] Zhang R, Yao E. Eco-driving at signalised intersections for electric vehicles. IET Intelligent Transport Systems 2015; 9(5): 488–497. https://doi.org/10.1049/iet-its.2014.0145 .

[11] Flehmig F, Sardari A, Fischer U, Wagner A. Energy optimal adaptive cruise control during following of other vehicles. 2015 IEEE Intelligent Vehicles Symposium (IV), Seoul, 2015, pp. 724-729. https://doi.org/10.1109/IVS.2015.7225770.

[12] Autonomie. https://www.autonomie.net/; Accessed 1 March 2019.

[13] Gao Z, Smith DE, Daw CS, Edwards KD, Kaul BC, Domingo N, et al., The evaluation of developing vehicle technologies on the fuel economy of long-haul trucks. Energy Conversion and Management 2015; 106:766-781. https://doi.org/10.1016/j.enconman.2015.10.006 .

[14] Gao Z, LaClair TJ, Smith DE, Daw CS. Exploring fuel-saving potential of long-haul truck hybridization. Transportation Research Record: Journal of the Transportation Research Board 2015; 2502: 99-107. https://doi.org/10.3141/2502-12 .

[15] Burress T. Benchmarking state-of-the-art technologies, https://www.energy.gov/sites/prod/files/2014/03/f13/ape006_burress_2013_o.pdf; 2018 [Accessed 20 September 2018].

[16] Gao Z, Lin Z, Franzese O. Energy consumption and cost savings of truck electrification for heavy duty vehicle applications. Transportation Research Record: Journal of the Transportation Research Board 2017; 2628: 99-109. http://dx.doi.org/10.3141/2628-11.

[17] Gao Z, Lin Z, Davis SC, Birky AK. Quantitative evaluation of MD/HD vehicle electrification using statistical data. Transportation Research Record: Journal of the Transportation Research Board 2018; 2672(24): 109-121. https://doi.org/10.1177/0361198118792329.

[18] Daw CS, Gao Z, Smith DE, LaClair TJ, Pihl JA, Edwards KD. Simulated fuel economy and emissions performance during city and interstate driving for a heavy-duty hybrid truck. SAE International Journal of Commercial Vehicles 2013; 6(1): 161-182. https://doi.org/10.4271/2013-01-1033.

[19] Gao Z, Kim MY, Choi JS, Daw CS, Parks JE, Smith DE. Cold-start emissions control in hybrid vehicles equipped with a passive hydrocarbon and NOx adsorber. Proc. IMechE–Part D: Journal of Automobile

Engineering 2012; 226(10): 1396-1407. https://doi.org/10.1177/0954407012443764.

[20] Gao Z, Daw CS, Wagner RM, Edwards KD, Smith DE. Simulating the impact of premixed charge compression ignition on light-duty diesel fuel economy and emissions of particulates and NOx. Proc. IMechE–Part D: Journal of Automobile Engineering 2013; 227(1): 31-51. https://doi.org/10.1177/0954407012459137.

[21] Gao Z, LaClair TJ, Daw CS, Smith DE, Franzese Q. Simulations of the fuel economy and emissions of hybrid transit buses over planned local routes. SAE International Journal of Commercial Vehicles 2014; 7(1): 216-237. https://doi.org/10.4271/2014-01-1562.

[22] Gao Z, Finney C, Daw C, LaClair T, Smith D. Comparative study of hybrid powertrains on fuel saving, emissions, and component energy loss in HD trucks. SAE International Journal of Commercial Vehicles 2014; 7(2): 414-431. https://doi.org/10.4271/2014-01-2326.

[23] Gao Z, Curran SJ, Parks JE, Smith DE, Wagner RM, Daw CD, et al. Drive cycle simulation of high efficiency clean combustions on fuel economy and exhaust properties in light-duty vehicles. Applied Energy 2015; 157: 762-776. https://doi.org/10.1016/j.apenergy.2015.03.070.

# Authors

Dr. Zhiming Gao is a R&D staff member at the National Transportation Research Center (NTRC) at Oak Ridge National Laboratory (ORNL). He has over 15 years of experience in fuel economy and emissions control related to advanced vehicle technologies, particularly in the field of vehicle component and powertrain simulation and modeling. His recent work focuses on vehicle electrification and connected and automated vehicle technologies for light-duty and heavy-duty vehicles. Dr. Gao has published more than 100 journal/conference papers, reports and presentations on combustion engines, aftertreatment, vehicle powertrains and CAV technologies.

Dr. Tim LaClair is a Research Staff Member at the Center for Transportation Analysis at ORNL. His work combines experimental measurement with computer modeling and analysis of data. Research activities during his 10 years at ORNL have focused largely on vehicle fuel efficiency, including the effects of different driving conditions and driver style as well as evaluating the benefits of advanced vehicle technologies. Recent research has focused on efficiency-oriented CAV systems. Dr. LaClair received a Bachelor's degree in Mathematics from the University of Michigan, a Master's degree in Mechanical Engineering from Florida Institute of Technology and a Ph.D. in Mechanical Engineering from Purdue University.